

Chapter 2

Locally Resonant Structures for Low Frequency Surface Acoustic Band Gap Applications

Abdelkrim Khelif, Younes Achaoui, and Boujemaa Aoubiza

Abstract In this chapter we investigate the propagation of acoustic waves in a two-dimensional array of cylindrical pillars on the surface of a semi-infinite substrate. Through the computation of the acoustic band diagram and transmission spectra of periodic pillars arranged in different symmetries, we show that these structures possess acoustic metamaterial features for surface acoustic waves. The pillars on the top of the surface introduce new guided modes in the non-radiative region of the substrate outside the sound cone. The modal shape and polarization of these guided modes are more complex than those of classical surface waves propagating on a homogeneous surface. Significantly, an in-plane polarized wave and a transverse wave with sagittal polarization appear that are not supported by the free surface. In addition, the band diagram of the guided modes defines band gaps that appear at frequencies markedly lower than those expected from the Bragg mechanism. We identify them as originating from local resonances of the individual cylindrical pillar and we show their dependence on the geometrical parameters, in particular with the height of the pillars. The frequency positions of these band gaps are invariant with the symmetry, and thereby the period, of the lattices, which is unexpected in band gaps based on Bragg mechanism. However, the role of the period remains important for defining the non-radiative region limited by the slowest bulk modes and influencing the existence of new surface modes of the structures. The surface acoustic wave transmission across a finite array of pillars corroborates the signature of

A. Khelif (✉)

International Joint Laboratory, GeorgiaTech-CNRS UMI 2958, 2-3 Rue Marconi, 57070 Metz, France

e-mail: abdelkrim.khelif@femto-st.fr

Y. Achaoui

Institut FEMTO-ST, Université de Franche-Comté, CNRS, 32 avenue de l'Observatoire, 25044 Besançon, France

e-mail: younes.achaoui@femto-st.fr

B. Aoubiza

Laboratoire de Mathématiques, Université de Franche-Comté, route de Gray, 25030 Besançon Cedex, France

e-mail: boujemaa.aoubiza@univ-fcomte.fr

the locally resonant band gaps for surface modes and their link with the symmetry of the source and its polarization. Numerical simulations based on an efficient finite element method and considering Lithium Niobate pillars on a Lithium Niobate substrate are used to illustrate the theory.

2.1 Introduction

The propagation of acoustic and elastic waves in inhomogeneous media has attracted a lot of interest during the last two decades. Usually presented as periodic structures with spatially modulated elastic moduli and mass density, the so-called phononic crystals have a number of important features such as the occurrence of frequency band gaps [13, 19]. In the frequency band gap ranges, sound and acoustic vibrations are strictly prohibited to propagate within these media resulting in a significant attenuation in their transmission spectra regardless of the direction of propagation. In order to widen these acoustic band gaps, different combinations of materials using solid/solid, solid/fluid and fluid/fluid phononic crystals have been put forward [11, 15, 20]. Using the band gap principle, phononic crystals allow the propagation of elastic or acoustic waves to be regulated. In other words, they play the role of perfect mirrors for elastic or acoustic waves in the frequency range of the band gap. The fundamental interest in controlling the elastic energy, and the potential applications, of phononic crystals are thus well established. These first studies of bulk, surface and Lamb waves have paved the way in establishing the fundamental physics in terms of controlling acoustic waves by trapping, guiding and demultiplexing them through single and linear defects [10, 12, 17].

Basically, band gaps can originate from Bragg reflections due to the periodicity of the structure. In this case, the spatial period of the crystal is of the same order of magnitude as the acoustic wavelength at the central frequency of the gap and, as a consequence, the lattice constant has generally been the key parameter to scale band gaps. A shortcoming of this principle was identified early in the context of low frequency acoustic applications for sound isolation, as well as earthquake shielding, which has long been regarded as a pernicious form of environmental pollution and a dangerous natural issue. In fact, complete sound attenuation for a low frequency range (10 Hz–10 KHz) needs a feature-sized structure of a few meters in order to ensure a spectral band gap with classical phononic crystals.

Another approach to realize low frequency acoustic band gaps, while utilizing lattice constants much shorter than the acoustic wavelength, is to use an acoustic metamaterial. More generally, these acoustic metamaterials are defined as an arrangement of artificial structural elements, designed to achieve advantageous and unusual acoustic properties and have an inhomogeneity scale that is much smaller than the wavelength of interest. Their acoustic response can be expressed in terms of homogenized material parameters. Various artificially engineered metamaterials are now demonstrating unprecedented acoustic proprieties that are not observed in naturally occurring materials. Among them are negative refraction, super-prism resolution, sub-wavelength acoustic imaging and acoustic cloaking. The structural

units of metamaterials can be tailored in shape and size, their composition and morphology can be artificially tuned, and inclusions can be designed and placed in a predetermined manner to achieve prescribed functionalities.

The first acoustic metamaterials appearing in the literature were so-called locally resonant sonic crystals [14] with acoustic resonators built into individual unit cells. The development of these acoustic metamaterials has led to groundbreaking demonstrations of the mass density law, often used in sonic shielding. Particularly, a broad frequency (10 Hz–10 KHz) sonic band gap with lattice constants two orders much shorter than the acoustic wavelength. The physical interpretation of locally resonance band gaps can result from the Fano resonance of a localized state with a continuum of propagation modes [5, 16]: at resonance, the energy of waves propagating in the matrix can be efficiently stored and delayed, while at anti-resonance, wave propagation becomes prohibited. In addition, the local resonance can be tuned by using intrinsic material features such as silicon rubber for which the sound velocity is two orders of magnitude lower than the one of the host matrix. For such composites, polarization-dependent frequency band gaps were reported for bulk waves [21] and complete band gaps were reported for Lamb waves [6]. A local resonance can also be altered using shape-design as in the case of Helmholtz resonators [4].

In this chapter, we consider a two-dimensional distribution of a periodic array of the pillars on the surface of a semi-infinite medium with different symmetries. The pillars are acting as local acoustic resonances interacting with the substrate continuum [1, 8, 18] and lead to the possibility of finding a low-frequency band gap for acoustic waves guided by the surface. In addition, we study the effect of square, triangular and honeycomb lattices on the band gaps. We highlight the role of the pitch, where it can be fundamental in controlling the dispersion of guided modes by defining the non radiative region and its non influence on the band gaps. The exhibition of these two features—the subwavelength low frequency band gaps and invariance with the lattice symmetries—makes the proposed structure an acoustic metamaterial. The numerical results presented here are related to the case of Lithium Niobate pillars on a Lithium Niobate substrate, but the conclusions remain valid for other materials and compositions as well. The chapter is organized in three sections. Section 2.2 deals briefly with model and method of calculation. In Sect. 2.3, we expose and discuss the main results of new surface modes and low frequency band gaps of different symmetry arrays. The conclusion is presented in Sect. 2.3.4.

2.2 Model and Method of Calculation

As illustrated in Fig. 2.1, we consider square, triangular and honeycomb lattice arrays of cylindrical pillars on the surface of a semi-infinite substrate. The z axis is chosen to be perpendicular to the surface and parallel to the cylinder axis. The lattice parameter of the acoustic periodic structure is a for square and triangular lattices and $\sqrt{3}a$ for honeycomb lattice. The filling fractions in the case of a square, triangular and honeycomb lattices, are respectively defined as: $F = \pi r^2/a^2$, $F = 4\pi r^2/\sqrt{3}a^2$

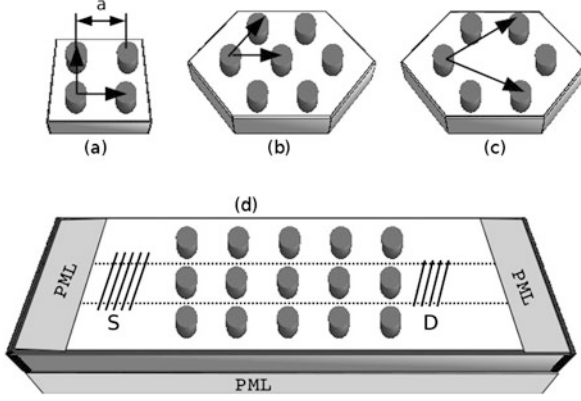


Fig. 2.1 Phononic periodic structure composed of cylindrical pillar arrays on a substrate with different symmetries: (a) square, (b) triangular and (c) honeycomb lattice. The lattice parameter is a for square and triangular lattices and $\sqrt{3}a$ for the honeycomb lattice. The pillars have height h and radius r . (a) The unit cell domains used for band structure calculations are meshed in three dimensions and Bloch-Floquet periodic boundary conditions are applied in both the x and the y directions. (b) The domain used for transmission computations has periodic boundary conditions along the y direction and a finite extent along the x direction. Perfectly matched layers are used to prevent reflections from the domain boundaries. A line S generates waves propagation in the (x, y) plane including surface acoustic waves. A line D detects the surface waves traveling through the finite size structure

and $F = (8\pi/3)r^2/\sqrt{3}a^2$. Here r is the radius of the cylinder and the height of the cylinders is h . Dispersion curves are calculated for the infinite system by using a finite element method in which only the unit cell is meshed and Bloch-Floquet conditions are implemented via periodic boundary conditions [9]. A three-dimensional mesh is used and the structure is assumed to be infinite and periodic in both the x and y directions (Fig. 2.1a). A phase relation is applied on the lateral sides of the mesh, defining boundary conditions between adjacent cells. This phase relation is related to the Bloch wave number of the modes of the periodic structure. By varying the wave vector in the first Brillouin zone and solving a spectral problem, the eigenfrequencies are obtained. The eigenvectors represent the modal displacement fields.

To simulate the transmission spectra through a finite size structure (finite number of periods), we use the model depicted in Fig. 2.1b. An incident surface acoustic wave with a specific polarization (u_x, u_z, u_y) is modelled by applying a line source vibrating on the surface. We apply in the y direction a periodic boundary condition that renders the line source infinitely long. The line source thus generates waves propagating in the (x, z) plane with uniform phase fronts along the y direction. In the far field of the source, the generated waves can be either bulk waves propagating away inside the substrate or surface waves propagating along the surface in the x direction. We assume that a few wavelengths from the source, the displacements at the surface are only caused by surface waves and not by bulk waves. To prevent reflections caused by the scattering of waves from the domain boundaries, perfectly

matched layers (PMLs) [2] are applied as illustrated in Fig. 2.1d. PMLs have the property that the mechanical disturbances are gradually absorbed in the layers before they can reach the outer boundaries [3]. Indeed, we can write the governing equation as

$$\frac{1}{\gamma_j} \frac{\partial T_{ij}}{\partial x_j} = -\rho \omega^2 u_i, \quad (2.1)$$

where ρ is the mass density of the material and ω is the angular frequency. Summation over repeated indices is implicitly assumed. T_{ij} is the stress tensor, the u_i are the displacements and the x_j are the coordinates ($x_1 = x$, $x_2 = y$, $x_3 = z$). The functions $\gamma_j(\mathbf{r})$ are the artificial damping along axis x_j at an arbitrary position \mathbf{r} inside the PML. As PMLs are added to attenuate acoustic waves propagating in the (x, z) plane, only γ_1 and γ_3 are different from 1. γ_1 is for instance given by

$$\gamma_1(x_1) = 1 - i\sigma_1(x_1 - x_l)^2, \quad (2.2)$$

where x_l is the coordinate of the interface between the regular domain and the PML and σ_1 is a suitable constant. There is no damping outside the PMLs and here $\gamma_j = 1$ is assumed. A suitable thickness of the PML as well as the value of σ_j must be found by trial calculations such that mechanical disturbances are absorbed before reaching the outer boundaries. However, the absorption variation must also be sufficiently slow so that reflections occurring at the interface between the regular domain and the PML are kept minimal. The mechanical stresses T_{ij} further depend on the strains as

$$T_{ij} = C_{ijkl} S_{kl}, \quad (2.3)$$

where the C_{ijkl} are the elastic stiffness constants. Strains are related to the displacements according to

$$S_{ij} = \frac{1}{2} \left(\frac{1}{\gamma_j} \frac{\partial u_i}{\partial x_j} + \frac{1}{\gamma_i} \frac{\partial u_j}{\partial x_i} \right). \quad (2.4)$$

2.3 Results and Discussion

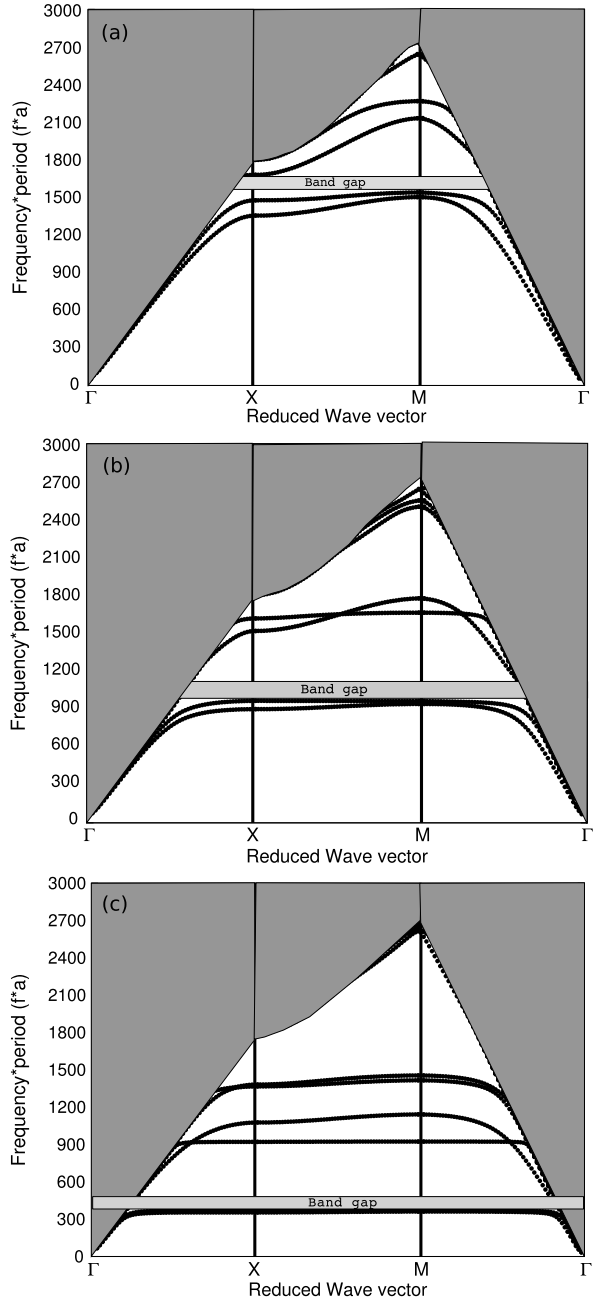
In this section, we discuss the effect of locally resonant modes of the pillars on surface waves of the substrate and the appearance of band gaps. These band gaps for the surface guided modes are restricted in a similar manner to those of photonic crystal slabs. Indeed, there is a continuum of radiation states that are extended infinitely in the region outside the slab [7]. Guided modes, which are states localized to the plane of the slab, can only exist in the regions of the band diagram that are outside the sound cone. Similarly, since the array of pillars we consider sits on top of a semi-infinite medium, the continuum of radiation states in this medium forms a sound cone. Guided acoustic waves, localized in the pillar array and the immediate vicinity of the substrate surface, can only exist in the regions of the band diagram that are outside the sound cone. However, this situation is unlike acoustic band

gaps of phononic crystal slabs, which may not be obvious at first sight. Phononic crystals slabs surrounded by a vacuum provide a naturally perfect confinement of waves in the vertical direction and their in-plane band gaps are similar to those of three-dimensional phononic crystals [14]; these band gaps are very sensitive to the existence of additional branches originating from the finite thickness of the slab [9]. In the following, we restrict our definition of band gaps to a range of frequencies in which no guided modes exist.

2.3.1 Band Diagram of Locally Resonant Surface Guided Modes

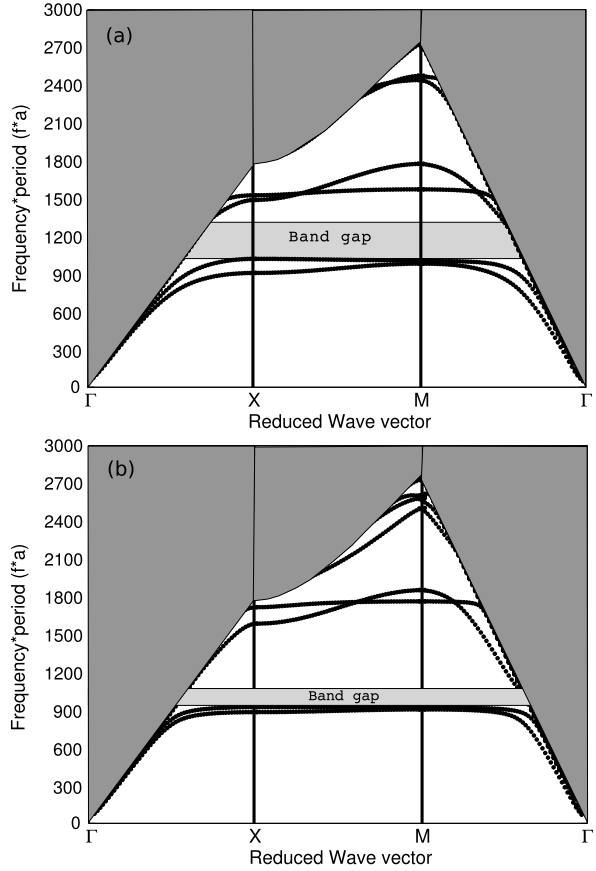
Obviously, the first parameter which can play an important role on the discrete acoustic modes of the pillars is their height. In order to investigate its influence, we have calculated the band diagram, for the guided modes, with a square lattice of the phononic crystal depicted in Fig. 2.1a. Propagation is in the (x, y) plane, and band structures are generated along the high symmetry axes of the first Brillouin zone. Both the substrate and the pillars are made from *Ycut* Lithium Niobate. A low filling fraction $F = 32\%$ ($r/a = 0.32$) and different relative heights of the cylinders ($h/a = 0.32, 0.5$ and 1.0) were considered for square lattice in Fig. 2.2. The gray region on the band structure is the sound cone representing the radiative zone of the Lithium Niobate substrate. The sound line limiting the sound cone is computed from the smallest phase velocity in the substrate as a function of the propagation direction. Due to the anisotropy of bulk acoustic wave propagation in Lithium Niobate, the sound line varies continuously along the XM direction of the first Brillouin zone. These particular choices for h/a ensure the existence of several absolute band gaps for guided modes. Particularly, in Fig. 2.2a when h/a is equal to 0.32 , two branches exist in the non radiative zone starting from zero frequency. The quasi-linear behavior of the mode dispersion is close to that of the classical surface acoustic waves except at the first limit of the Brillouin zone. Indeed, at the X point of the reduced wave vector the two branches are folded back due to the array period and their interaction induced the first band gap operating from $fa = 1600$ to 1700 m/s. The frequency positions of the band gap are very close to those expected from Bragg interferences related to the pitch period. Which means that the pillars act here to slow the surface wave velocity as is usual in phononic crystals and their discrete acoustic modes do not erupt in the non radiative zone. When the height of the pillars is increased, the branches shift down towards low frequencies and other kinds of band gaps show up. In fact, for $h/a = 0.5$, we find two band gaps extending, respectively, from $fa = 1000$ to 1100 m/s and a very narrow band gap appearing around the radiation limit in ΓX direction, i.e. $fa = 1700$ m/s. Moreover, with equality of height and period $h/a = 1.0$ as a condition, the first band gap occurs at a central frequency of $fa = 400$ m/s and its relative bandwidth reaches 22% . A wider second band gap appears around $fa = 1550$ m/s. The first band gap (low frequency) is bounded from below by flat branches, which induce zero group velocities and space confinement of the acoustic energy. This effect outlines the role

Fig. 2.2 Band structure of a square array of cylindrical pillars on a Lithium Niobate substrate, calculated along high symmetry directions of the first irreducible Brillouin zone. The lattice parameter is a and the filling fraction $F = 0.3$. The relative height of the cylinders h/a equals (a) 0.32, (b) 0.5, and (c) 1.0. The gray region represents the sound cone of the substrate. The sound line limiting the sound cone is given by the smallest phase velocity in the substrate for every propagating direction



of the locally resonant modes of the pillars. The frequency position of the first band gap is markedly lower, and the wavelength propagating in the surface is one order

Fig. 2.3 Same parameters as Fig. 2.2, but instead two values of the filling fraction are compared: (a) $F = 0.4$ and (b) $F = 0.25$



greater, than the period of the structure. Finally, the pitch period and the filling fraction are kept fixed in Fig. 2.2, which clearly shows that the origin of the band gaps is not related to Bragg interferences, as in classic phononic crystals, but is rather related to the result of resonant modes of the structure.

Usually the other important geometrical parameter in the process of opening band gaps and controlling their bandwidths is the filling fraction F . We plot in Fig. 2.3 the band diagram for two values of filling fraction $F = 0.25$ and 0.4 . The relative height h/a is fixed to 0.5 which allows us to compare the results with those of Fig. 2.2b. The increase of the filling fraction to $F = 0.4$, as compared to $F = 0.32$, induces a relative widening of the band gap. In fact, when the filling fraction is increased, or the space between adjacent pillars is reduced, the interaction between locally resonant modes can be enhanced through surface coupling and can lead to wider band gaps. Besides, we observe that the second and the fourth bands are more sensitive to the filling fraction. In the opposite case, decreasing the filling fraction, the band gap becomes smaller. However, the central frequency position is not very sensitive to the filling fraction as is usual in any phononic crystal systems.

In general, if h/a is smaller than 0.3, the acoustic modes of the pillars appear at well separated frequencies within the sound cone and thus radiate into the bulk. However, when h/a is increased, the acoustic modes of the pillars shift down in frequency. They are then in a position to interact and form collective propagating surface modes, whereby acoustic energy can be guided along the surface of the substrate. Concurrently, this interaction opens band gaps inside which guided surface acoustic waves are forbidden to propagate. The band gaps shown in Fig. 2.2 are complete and omnidirectional for guided modes at the surface of the substrate. Such guided waves exist only under the sound cone such as, for instance, the Rayleigh surface wave of the homogeneous surface. This means that when a standard Rayleigh surface wave propagating on the free surface of the substrate is incident on the pillar array, it will be either converted to the existing surface-pillar modes at the same frequency, or reflected from the array if the frequency is within a band gap for guided waves. Naturally, a fraction of the surface wave energy can be converted to radiation modes of the substrate at the phononic crystal boundary in both cases, but this does not preclude that no energy is propagated along the surface within a band gap for guided waves. This exhibition of band gaps makes the pillars a very appealing structure in achieving low frequency applications with lattice constants much shorter than the acoustic wavelength.

2.3.2 Wave Transmission of Locally Resonant Surface Guided Modes

It is well known that the study of wave transmission in finite size systems is crucial in understanding the size effect (number of periods) on the band gap attenuations, insertion loss and reflection spectra; this is especially so when the structures possess a radiation condition, which is the case in 1D and 2D periodic systems. For instance, in our case the radiative zone allows the surface waves to leak into the bulk. However, the evaluation of the leaks is not obvious from the band diagram. In the following, we describe the wave transmission properties through a finite number of pillars on the substrate.

The wave transmission spectra were simulated for propagation along the x direction, using the three dimensional domain depicted in Fig. 2.1d. The domain is finite along x with seven rows of pillars sandwiched between the incoming and the outgoing media and infinitely periodic along y . A line source is applied on the surface of the Lithium Niobate substrate just in front of the first pillar. This source vibrates at a monochromatic frequency and can have two different polarizations: either (i) (u_x, u_z) sagittal displacements, which can excite the Rayleigh surface wave of the homogeneous surface or (ii) u_y transverse displacements which can be considered as a shear horizontal wave source. Basically, most elastic materials with free surface (i.e., without phononic crystal) do not support the propagation of the shear horizontal surface wave. Nevertheless, the periodic array of pillars can support surface modes with such a polarization, as discussed in the following.

Fig. 2.4 Band diagram for surface guided waves propagating along the ΓX direction with a square-lattice phononic crystal composed of cylindrical Lithium Niobate pillars on a Lithium Niobate substrate. The filling fraction is equal to $F = 0.3$ and the relative height is fixed to $h/a = 0.5$. Transmission of surface waves through 7 rows: ((a) *straight line*) Computed transmission spectrum with a sagittally polarized excitation line source. ((b) *dashed line*) Computed transmission spectrum with a shear horizontally polarized excitation line source. Transmissions represent an average of all displacement components, $|u_x| + |u_z| + |u_y|$, as a function of frequency. The average is collected along a line D (see Fig. 2.1) located after the seventh period of pillars

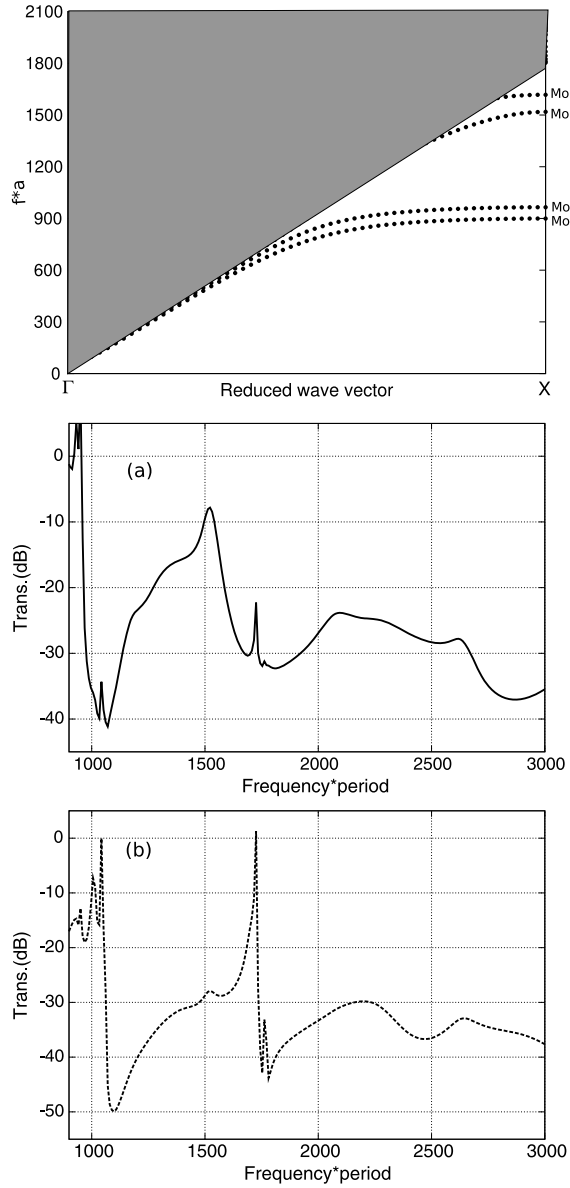
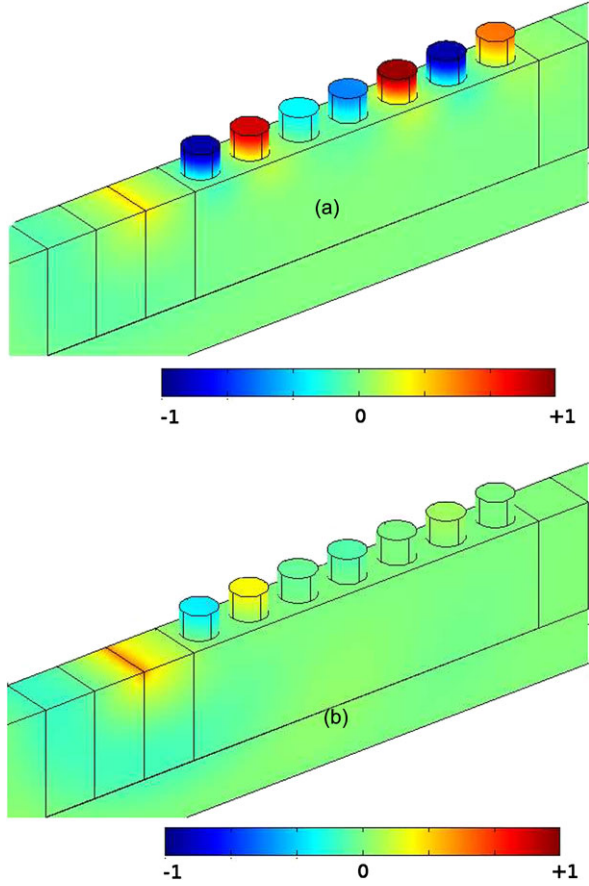


Figure 2.4 display the computed transmissions for the sagittal and the shear horizontal line sources. The band diagram is added to the transmission to help in interpretation of the results. The filling fraction is fixed to $F = 0.32$ and the relative height of the pillars is $h/a = 0.5$. Transmissions are computed for the ΓX direction of the band diagram. The transmission in Fig. 2.4a is for the total displacement, but is however related to the sagittal (u_x, u_z) excitation. Two attenuations are apparent in the transmission. The first drop is centered at $f a = 1050$ m/s corresponding to

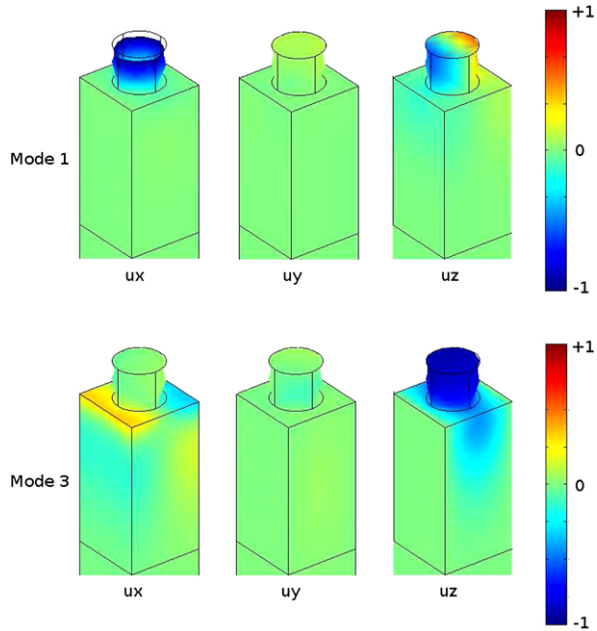
Fig. 2.5 Computed displacement field $|u_y|$ with a shear horizontal polarized excitation line source.
 (a) displacement field at resonance frequency.
 (b) displacement field at anti-resonance frequency



the first and the third band limits in the band diagram. The second drop centered at $fa = 1700$ m/s is related to the third band and the limit of the non radiative zone. Besides, the computed transmission for the shear horizontal line source in Fig. 2.4c displays two narrow pass bands occurring at $fa = 1050$ m/s and 1700 m/s. These frequency positions correspond to the deep attenuations of sagittal excitation shown in Fig. 2.4b. The response of the different excitations allows us to suggest that the second and the fourth branches are deaf to the sagittal source while the first and the third bands are deaf to the shear horizontal source.

In addition, the shape of the transmission for the shear horizontal source around the frequencies where the second and fourth bands reach the X point is typical of a linear response function proportional to $1/(f_0^2 - f^2)$, when a wave with frequency f interacts with a medium supporting a localized excitation with frequency f_0 . Such an effect is manifest, for instance, in the electromagnetic frequency response of materials with optical resonances or more generally the so-called Fano resonances of a localized state interacting with a continuum of propagating modes. In order to have a physical interpretation of these local resonances, we display in Figs. 2.5a and 2.5b

Fig. 2.6 Eigenmode of mode 1 and mode 3 analysis close to the point X of the Brillouin zone. They represent the displacement field of the three components u_x and u_z and u_y . These modes have mostly in-plane polarization

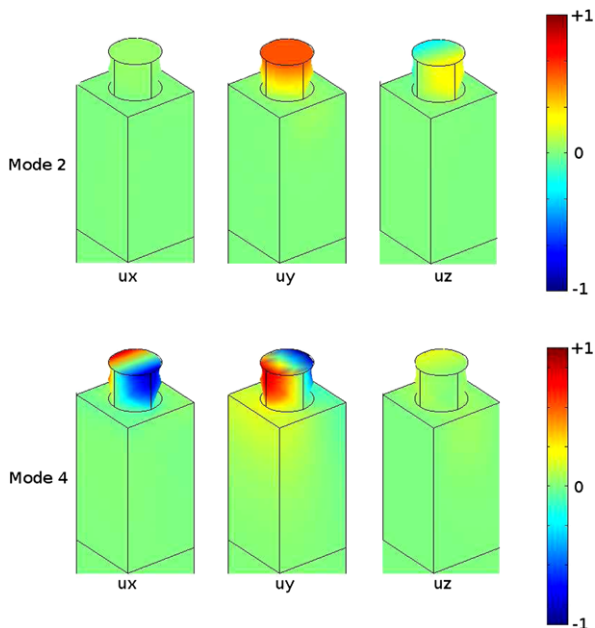


the displacement field $|u_y|$ of the transmission for two significant frequencies—resonance and anti-resonance—occurring at $fa = 1042$ m/s and $fa = 1100$ m/s. In Fig. 2.5a, the energy of waves propagating in the matrix can be efficiently stored in the pillars and delayed at the resonance frequency $fa = 1042$ m/s corresponding to the maximum transmission in Fig. 2.4c. However, at the anti-resonance frequency $fa = 1100$ m/s which corresponds to a strong attenuation in the transmission spectra, the wave propagation becomes prohibited and the pillars act as an obstacle for the guided wave in Fig. 2.5b. Naturally, a fraction of the surface wave energy can be converted to radiation modes of the substrate at the structure boundary in both cases, but this does not preclude that no energy is propagated along the surface within a band gap for guided waves.

To corroborate the previous observations of deaf bands, we plot in Figs. 2.6 and 2.7 the modal displacements of the first and the third bands, and on the second and fourth bands, respectively. The wavevector k_x selected for these illustrations is close to the point X of the first Brillouin zone. We emphasize that the acoustic energy is mostly distributed between u_x and u_z for the eigenmodes in Fig. 2.6. Those modes have mostly sagittal polarization. The displacement u_y is not equal to zero but is very small in comparison. We notice that the same scale has been used in all displacements to give a good appreciation of each polarization. This observation explains the significant transmission magnitude of the first and the third bands with the a sagittal source.

As Fig. 2.7 shows, the acoustic energy is mostly distributed between u_z and u_y for the second band and between u_x and u_y for the fourth band. We observe that the u_z displacement for the second band and the u_x displacement for the fourth band

Fig. 2.7 Same as Fig. 2.6 for mode 2 and mode 4, these modes have mostly sagittal polarization with transverse propagation

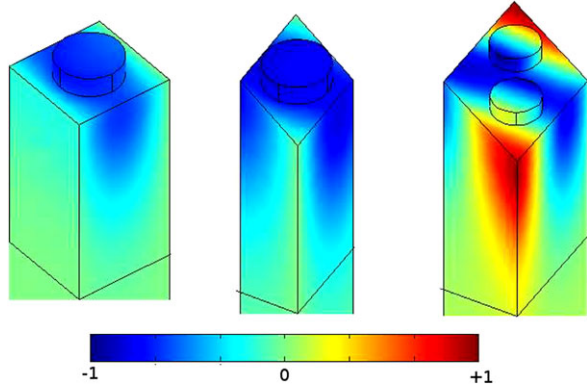


have an antisymmetric character with respect to the sagittal mid plane (x, z) of the structure. The sagittal excitation is symmetric with respect to the same mid-plane, which means that the energy cannot be transferred to the second and the fourth bands. This explains the absence of a signature of these modes in the transmission spectra with the sagittally polarized source. Conversely, the u_y displacement is symmetric with respect to the sagittal mid plane and can thus be excited by the shear horizontally polarized source.

2.3.3 Lattice Symmetry Effect on the Locally Resonant Surface Acoustic Band Gaps

Basically, in metamaterial structures the observed phenomena are not linked to the period pitch or to the lattice symmetries and can appear in disordered systems, on the strict condition that the local resonances are not affected. Aiming to highlight this effect, we describe in this section the effect of the surface acoustic wave propagation properties of pillars on semi-infinite substrate with square, triangular and honeycomb lattices. Especially, we focus on the position of the locally resonant band gap in respect to these symmetry lattices. In other words, we wish to demonstrate that the sub-wavelength band gaps are not sensitive to the period pitch—which can be found in conventional phononic crystals—and reinforce the position of this structure as an acoustic metamaterial element. However, the considered pitch will

Fig. 2.8 Eigenmode of the lowest frequency mode analysis close to the limit of the first Brillouin zone for the square, triangular and honeycomb symmetries. These are the total displacement field of the three component u_x and u_z and u_y . The relative radius is $r/a = 0.32$ and the relative height of the cylinders h/a equals 0.2



play a fundamental role in controlling the dispersion of guided modes and will define the non radiative zone which is a key condition to obtain guided modes.

As discussed in Sect. 2.2, when the discrete acoustic resonances of the pillars are not able to appear in the non-radiative zone due to the small value of the pillars height h/a , we still have two major effects coming from the presence of pillars: the existence of two surface waves propagating in the substrate with different polarizations and a slowing down of the classical wave velocity of the substrate. The latter effect is less pronounced in the case of the honeycomb structure. In fact, the pitch is larger than the other symmetries ($\sqrt{3}a$) which decreases its filling fraction, and therefore reduces the slowing down effect of the classical surface wave. Figs. 2.8a, b and c show the field distribution of the total displacement close to the limit of the first Brillouin zone for the square, triangular and honeycomb symmetries respectively. The relative radius is $r/a = 0.32$ and the relative height of the cylinders h/a equals 0.2. These modes have different shape for the three symmetries and cover both the pillar and the surface of the substrate. Consequently, the period pitch will affect the wave propagation properties through the phase condition that can be applied in each different symmetry lattice.

Actually, the relative height of the pillars is fixed at $h/a = 0.6$ to ensure the presence of pillars vibration modes in the non radiative zone. As shown in Fig. 2.9, several bands appear below the sound cone and low frequency band gaps show up. We observe the existence of two band gaps appearing around $fa = 1150$ m/s and $fa = 2200$ m/s for square and triangular lattices (Figs. 2.9a and 2.9b). In the case of honeycomb lattice, only one complete band gap for guided modes opens around $fa = 1150$ m/s Fig. 2.9c. Although, there is a large difference between lattice pitch of square or triangular (a) and honeycomb ($\sqrt{3}a$), we highlight that the first band gaps appear at the same frequency position in the three different lattice symmetries. This means, that the physical phenomena behind the opening of the band gap is clearly not due to the Bragg interference of waves linked to the period, but to the signature of the locally resonance acoustic vibration of the pillars. The expectation of the same position of the band gap occurring in any other ordered or disordered structures is presumably upon condition that keeping the same geometry of pillars, which ensures the resonance frequency positions.

Fig. 2.9 Band structure of a phononic crystal composed of cylindrical lithium niobate pillars on a lithium niobate substrate, calculated along high symmetry directions of the first irreducible Brillouin zone for: (a) square; (b) triangular; (c) honeycomb. The lattice parameter is a for triangular and square lattice and $(\sqrt{3}a)$ for the honeycomb lattice. The radius is $r/a = 0.32$ and the relative height of the cylinders h/a equals 0.6. The gray region represents the sound cone of the substrate. The sound line limiting the sound cone is given by the smallest phase velocity in the substrate for every propagation direction

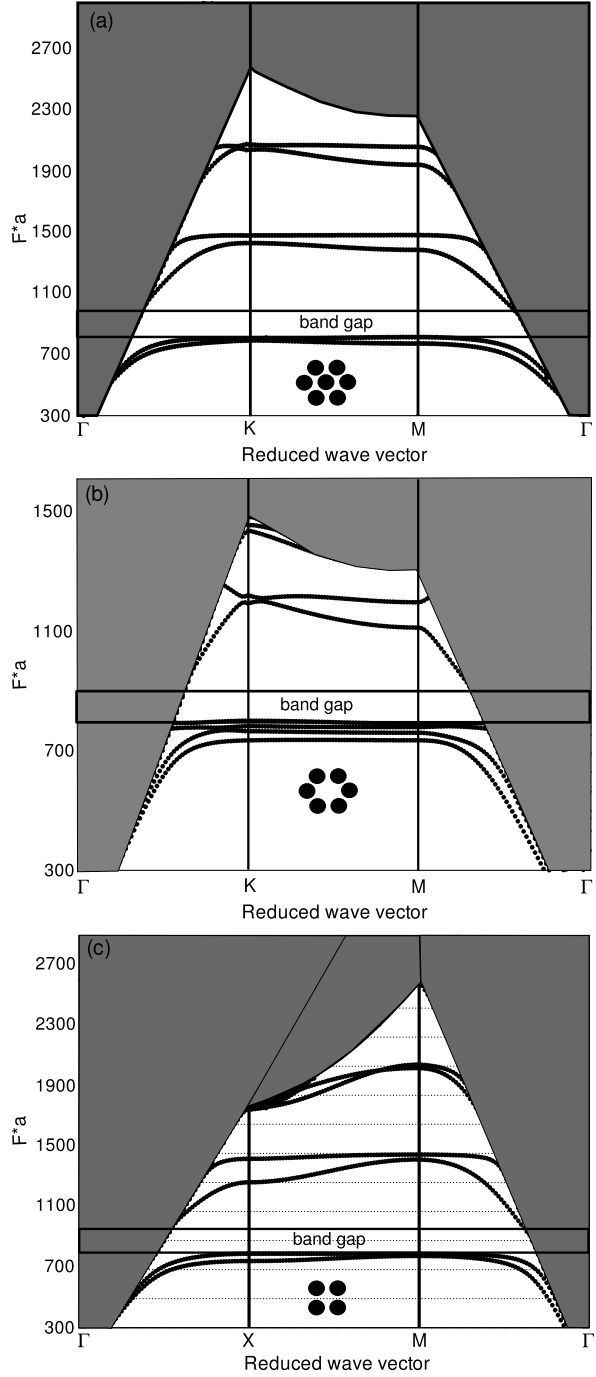
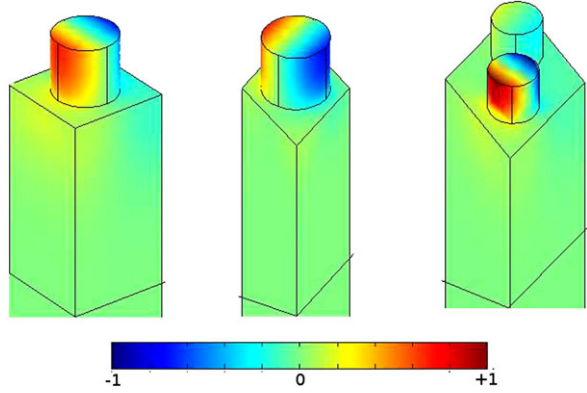


Fig. 2.10 Eigenmode of the lowest frequency mode analysis close to the limit of the first Brillouin zone for the square, triangular and honeycomb symmetries. These are the total displacement field of the three component u_x and u_z and u_y . These modes have mostly the same shape for the three symmetries. The relative radius is $r/a = 0.32$ and the relative height of the cylinders h/a equals 0.6



To corroborate this effect, we display in Fig. 2.10 the mode shapes of the lowest frequency solutions for the three lattices. The wave vectors of the eigenmodes are chosen close to the limit of the first Brillouin zone. These mode shapes, which represent the total displacement field of the three components u_x and u_z and u_y , have mostly the same shape for the three symmetries and demonstrate that the flat bands observed in their band diagrams are related to the discrete acoustic mode of the pillars.

2.3.4 Conclusion

In summary, the study of the locally acoustic resonances with different periodic arrays of cylindrical pillars deposited on a semi-infinite substrate is presented. The band structures of square, triangular and honeycomb arrays show that they possess the characteristics of acoustic metamaterials. Precisely, the presence of pillars introduce new surface propagating modes. The period defines the non-radiative region limited by the slowest bulk modes and influences the existence of these new modes. In addition, with a specific geometrical value of pillars, guided modes define a first band gap that appears at frequencies markedly lower than those expected from the Bragg condition and it does not depend on the symmetry of the arrays. This band gap originates from local resonances of the individual cylindrical pillars and is sensitive to their geometrical parameters, in particular to the height of the pillars. The transmission calculation corroborates very well with the band structure and highlights the major role of the local resonance of a single pillar in the opening of the low frequency band gap. In this case, we expect the same band gap position to occur in any other ordered or disordered structures.

Acknowledgements The authors thank Prof. Vincent Laude and Dr. Sarah Benchabane for fruitful discussions.

References

1. Achaoui, Y., Khelif, A., Benchabane, S., Robert, L., Laude, V.: Experimental observation of locally-resonant and Bragg band gaps for surface guided waves in a phononic crystal of pillars. *Phys. Rev. B* **83**, 104201 (2011)
2. Berenger, J.P.: A perfectly matched layer for the absorption of electromagnetic waves. *J. Comput. Phys.* **114**, 185 (1994)
3. Dühning, M.B., Laude, V., Khelif, A.: Energy storage and dispersion of surface acoustic waves trapped in a periodic array of mechanical resonators. *J. Appl. Phys.* **105**, 093504 (2009)
4. Fang, N., Xi, D., Xu, J., Ambati, M., Srituravanich, W., Sun, C., Zhang, X.: Ultrasonic metamaterials with negative modulus. *Nat. Mater.* **5**, 452 (2006)
5. Goffaux, C., Sánchez-Dehesa, J., Levy Yeyati, A., Khelif, A., Lambin, P., Vasseur, J.O., Djafari-Rouhani, B.: Evidence of Fano-like interference phenomena in locally resonant materials. *Phys. Rev. Lett.* **88**, 225502 (2002)
6. Hsu, J.C., Wu, T.T.: Lamb waves in binary locally resonant phononic plates with two dimensional lattices. *Appl. Phys. Lett.* **90**, 201904 (2007)
7. Johnson, S.G., Fan, S., Villeneuve, P.R., Joannopoulos, J.D., Kolodziejski, L.A.: Guided modes in photonic crystal slabs. *Phys. Rev. B* **60**, 5751–5758 (1999)
8. Khelif, A., Achaoui, Y., Benchabane, S., Laude, V., Aoubiza, B.: Locally resonant surface acoustic wave band gaps in a two-dimensional phononic crystal of pillars on a surface. *Phys. Rev. B* **81**, 214303 (2010)
9. Khelif, A., Aoubiza, B., Mohammadi, S., Adibi, A., Laude, V.: Complete band gaps in two-dimensional phononic crystal slabs. *Phys. Rev. E* **74**, 046610 (2006)
10. Khelif, A., Choujaa, A., Benchabane, S., Djafari-Rouhani, B., Laude, V.: Guiding and bending of acoustic waves in highly confined phononic crystal waveguides. *Appl. Phys. Lett.* **84**(22), 4400–4402 (2004)
11. Khelif, A., Choujaa, A., Djafari-Rouhani, B., Wilm, M., Ballandras, S., Laude, V.: Trapping and guiding of acoustic waves by defect modes in a full-band-gap ultrasonic crystal. *Phys. Rev. B* **68**, 214301 (2003)
12. Khelif, A., Wilm, M., Laude, V., Ballandras, S., Djafari-Rouhani, B.: Guided elastic waves along a rod-defect of a two-dimensional phononic crystal. *Phys. Rev. E* **69**, 067601 (2004). doi:[10.1103/PhysRevE.69.067601](https://doi.org/10.1103/PhysRevE.69.067601)
13. Kushwaha, M.S., Halevi, P., Dobrzynski, L., Djafari-Rouhani, B.: Acoustic band structure of periodic elastic composites. *Phys. Rev. Lett.* **71**(13), 2022–2025 (1993). doi:[10.1103/PhysRevLett.71.2022](https://doi.org/10.1103/PhysRevLett.71.2022)
14. Liu, Z., Zhang, X., Mao, Y., Zhu, Y.Y., Yang, Z., Chan, C.T., Sheng, P.: Locally resonant sonic materials. *Science* **289**, 1734 (2000)
15. Martínez-Sala, R., Sancho, J., Sanchez, J.V., Gomez, V., Llinares, J., Meseguer, F.: Sound attenuation by sculpture. *Nature* **378**, 241 (1995)
16. Miroshnichenko, A.E., Flach, S., Kivshar, Y.S.: Fano resonances in nanoscale structures. *Rev. Mod. Phys.* **82**(3), 2257 (2010). doi:[10.1103/RevModPhys.82.2257](https://doi.org/10.1103/RevModPhys.82.2257)
17. Pennec, Y., Djafari-Rouhani, B., Vasseur, J.O., Larabi, H., Khelif, A., Choujaa, A., Benchabane, S., Laude, V.: Acoustic channel drop tunneling in a phononic crystal. *Appl. Phys. Lett.* **87**(26), 261912 (2005). doi:[10.1063/1.2158019](https://doi.org/10.1063/1.2158019)
18. Robillard, J.F., Devos, A., Roch-Jeune, I.: Time-resolved vibrations of two-dimensional hypersonic phononic crystals. *Phys. Rev. B* **76**(9), 092301 (2007). doi:[10.1103/PhysRevB.76.092301](https://doi.org/10.1103/PhysRevB.76.092301)
19. Sigalas, M.M., Economou, E.N.: Band structure of elastic waves in two dimensional systems. *Solid State Commun.* **86**(3), 141–143 (1993)
20. Vasseur, J.O., Deymier, P.A., Chenni, B., Djafari-Rouhani, B., Dobrzynski, L., Prevost, D.: Experimental and theoretical evidence for the existence of absolute acoustic band gaps in two-dimensional solid phononic crystals. *Phys. Rev. Lett.* **86**(14), 3012–3015 (2001)
21. Wang, G., Wen, X., Wen, J., Shao, L., Liu, Y.: Two dimensional locally resonant phononic crystals with binary structures. *Phys. Rev. Lett.* **93**, 154302 (2004)

Acoustic Metamaterials

Negative Refraction, Imaging, Lensing and Cloaking

Craster, R.V.; Guenneau, S. (Eds.)

2013, XVI, 324 p., Hardcover

ISBN: 978-94-007-4812-5